

## Mixing and segregation in binary polar-molecule clusters

Valeria Molinero

*Departamento de Química Inorgánica, Analítica y Química Física, Facultad de Ciencias Exactas y Naturales, Universidad de Buenos Aires, Pabellón II, (1428) Capital Federal, Argentina*

Daniel Laria

*Departamento de Química Inorgánica, Analítica y Química Física, Facultad de Ciencias Exactas y Naturales, Universidad de Buenos Aires, Pabellón II, (1428) Capital Federal, Argentina and Unidad Actividad Química, Comisión Nacional de Energía Atómica, Av. del Libertador 8250, (1429) Capital Federal, Argentina*

Raymond Kapral

*Chemical Physics Theory Group, Department of Chemistry, University of Toronto, Toronto, Ontario M5S 3H6, Canada*

(Received 4 May 1998; accepted 23 July 1998)

Structural and dynamical properties of liquid-state, binary, water-acetonitrile nanoclusters are studied. When acetonitrile is the solute species, it exhibits a propensity to reside on the cluster surface, although one may identify regions interior to the cluster that are favorable for solvation. The dynamics of the interchange of acetonitrile between surface and interior solvation regions and structural aspects of surface solvation states are studied. When water is the solute it tends to be solvated in the interior of the cluster and form aggregates. The nature and dynamics of contact and solvent separated water pairs in these clusters is investigated, and the recombination dynamics of larger water aggregates in concentrated water-acetonitrile clusters is examined. © 1998 American Institute of Physics. [S0021-9606(98)51540-1]

### I. INTRODUCTION

Investigations of the properties of clusters with varying sizes and in various physical states constitute an active research area.<sup>1,2</sup> Cluster properties such as the solid-state structure of small aggregates,<sup>3</sup> solid-liquid phase transitions in small cluster systems,<sup>4-10</sup> reactions in clusters<sup>11-14</sup> such as proton transfer processes,<sup>15,16</sup> acid dissociation in aprotic aggregates,<sup>17</sup> excited-state dynamics in argon clusters,<sup>18</sup> spectral shifts of chromophores,<sup>19</sup> photoelectron spectroscopy of ions in water clusters,<sup>20</sup> nucleophilic substitution reactions,<sup>21</sup> electronic states in ionic clusters,<sup>22,23</sup> ionic states in polar aggregates,<sup>24-26</sup> cage dynamical effects that follow photodissociation processes,<sup>27-29</sup> to name a few examples, have been the topics of both experimental and theoretical studies.

Nanoscale clusters have properties which differ from both small aggregates composed of a few molecules and bulk phases. They are sufficiently large to exhibit bulklike phases, which often differ from those of infinite systems, yet surface forces play an important role in determining their properties. These effects have been demonstrated to play important roles in cluster reactions and solvation and are especially evident in binary liquid-state clusters where the mixing properties differ substantially from bulk binary fluids.<sup>30,31</sup>

The solvation structure and dynamics of solute molecules in binary, liquid-state nanoclusters is influenced by the interplay between surface and bulk forces. These effects are also responsible for the stabilization of surface and cluster-interior solvation species.<sup>24</sup> Strong structural correlations in the cluster interior are induced by the finite size and surface forces leading to bulk-like phases in the cluster that

differ from their infinite-system analogs. The distinctive structural features can give rise to solvent-stabilized species whose dynamics is, in turn, influenced by the system's finite size. These are some of the issues that are studied in this paper.

The focus is on liquid-state binary clusters composed of water and acetonitrile molecules. We have examined both the solvation structure and dynamics of these systems. The main objectives of this study were twofold: first, since both species exhibit a marked dipolar character, it is interesting to investigate how the details of the molecular forces and lack of translational symmetry affect the possible stable cluster morphologies. Second, water and acetonitrile exhibit important differences in their microscopic intramolecular connectivities; perhaps the most obvious is the absence of a hydrogen-bonded, three-dimensional network in the latter solvent. Although it is still possible to establish cross hydrogen bonding between both species, the fact that acetonitrile is aprotic leads to a clear asymmetry in the roles of these two species as potential proton donors or acceptors. One should expect that this asymmetry will be reflected in the structural features of "bulk" states and their interfaces, regardless of the particular cluster composition considered. These polar-molecule clusters have a richer structure than that of binary Lennard-Jones clusters.<sup>30,31</sup>

The outline of the paper is as follows. In Sec. II we give details of the model potentials and molecular dynamics simulation methods used in the study. Section III is devoted to the study of dilute binary clusters containing one or two solute molecules. The character of the solvation, surface vs cluster interior, and the existence of various solvent-

TABLE I. Parameters for the potentials.<sup>a</sup>

Site	$\sigma$ (Å)	$\epsilon$ (kcal mol <sup>-1</sup> )	Charge ( $e$ )
O	3.17	0.156	-0.820
H	0.00	0.000	0.410
C	3.40	0.099	0.129
CH <sub>3</sub>	3.60	0.380	0.269
N	3.30	0.099	-0.398

<sup>a</sup>Internuclear distances (Å):  $d_{\text{O-H}}=1.0$ ;  $d_{\text{H-H}}=1.633$ ;  $d_{\text{C-N}}=2.63$ ;  $d_{\text{C-CH}_3}=1.46$ ;  $d_{\text{N-CH}_3}=1.17$ . The usual geometrical and arithmetic means were used to determine the  $\epsilon$  and  $\sigma$  parameters for the cross interactions.

stabilized species is described. Section IV considers large, concentrated binary clusters. Both the nature and dynamics of the superficial and cluster-interior solvation states are described. For both dilute and concentrated binary clusters we find that the cluster properties differ significantly depending on whether water or acetonitrile is the solute. The conclusions of the study are given in Sec. V.

## II. MODEL AND SIMULATION METHOD

Simulations were performed on  $[n:m]$  clusters containing  $n$  molecules of acetonitrile (ACN) [CH<sub>3</sub>CN] and  $m$  molecules of water ( $W$ ). The component with the smaller (larger) mole fraction will henceforth be denoted as the solute (solvent). Water intermolecular interactions were described by the three-site SPC model of Berendsen *et al.*,<sup>32</sup> while ACN was modeled as a rigid three-site molecule comprising a united atom model for the CH<sub>3</sub> group, C and N units in a linear arrangement.<sup>33</sup> The potential energy of the entire system  $V_s$  was taken to be sum of pairwise additive contributions

$$V_s = \sum_{i < j} v(i, j). \quad (1)$$

The interaction potentials  $v(i, j)$  between the  $i$ th and  $j$ th molecules is the sum of Lennard-Jones terms between different interaction sites and Coulomb terms arising from the interactions between partial charges on the sites:

$$v(i, j) = \sum_{i'j'} [v_{i'j'}^{\text{LJ}}(|\mathbf{r}_{i'} - \mathbf{r}_{j'}|) + v_{i'j'}^{\text{C}}(|\mathbf{r}_{i'} - \mathbf{r}_{j'}|)], \quad (2)$$

where the sums are over all sites  $i'$  and  $j'$  in molecules  $i$  and  $j$ , with

$$v_{i'j'}^{\text{LJ}}(r) = 4\epsilon_{i'j'} \left[ \left( \frac{\sigma_{i'j'}}{r} \right)^{12} - \left( \frac{\sigma_{i'j'}}{r} \right)^6 \right], \quad (3)$$

and

$$v_{i'j'}^{\text{C}}(r) = \frac{z_{i'} z_{j'} e^2}{r}, \quad (4)$$

where  $\mathbf{r}_{i'}$  denotes the coordinate of site  $i' = \text{O, H, CH}_3, \text{N, C}$  in the  $i$ th molecule and  $e$  is the electron charge. Details of the energy and length parameters are given in Table I.

The molecular dynamics simulations consisted of an initial equilibration period of about 100 ps using Nosé canonical dynamics<sup>34</sup> at an average temperature of  $T \approx 200$  K. At

this temperature, the structural and dynamical properties of the clusters were similar to those of liquidlike phases. Subsequent to this equilibration period, the Nosé thermostat was switched off and statistics were collected from long (3–4 ns) constant energy trajectories. The Verlet algorithm<sup>35</sup> with a time step of 1 fs was used to integrate the classical equations of motion; with this time interval, the energy conservation was maintained below 0.1%. Intramolecular constraints in the solvent particles were implemented using the SHAKE algorithm.<sup>36</sup> Although the isolated molecular clusters under study are metastable since evaporation must eventually occur, little or no evaporation was observed on the 3–4 ns time scale of the simulations and well defined statistical averages could be determined from time averages over the trajectories.

## III. DILUTE BINARY CLUSTERS

We shall examine some general aspects of the solvation structure of binary molecular clusters. One of the gross features to consider is whether the solute molecules reside on average in the interior or near the surface of the cluster. A useful quantity to consider in this connection is the spatial correlation function of component  $\alpha = W$  or ACN with respect to the center of mass of the cluster,  $g_{\text{CM}-\alpha}(r)$ , defined as,

$$g_{\text{CM}-\alpha}(r) = \frac{1}{4\pi r^2 N_\alpha} \left\langle \sum_{i=1}^{N_\alpha} \delta(|\mathbf{R}_i^\alpha - \mathbf{R}_{\text{CM}}| - r) \right\rangle, \quad (5)$$

which gives the probability of finding a molecule of species  $\alpha$  at a distance  $r$  from the cluster center of mass. Here  $\mathbf{R}_i^\alpha$  denotes the center of mass of the  $i$ th molecule of species  $\alpha$  and  $\mathbf{R}_{\text{CM}}$  is the position of the center of mass of the cluster. The number of molecules of species  $\alpha$  is  $N_\alpha = n$  or  $m$ , while the angle brackets represent a time average over a microcanonical trajectory as discussed above.

We begin by studying one and two solute molecules of either species in the cluster and examine more concentrated binary clusters in the following section.

### A. [1:m] and [n:1] clusters

Consider a single ACN molecule in an  $m$ -molecule water cluster ([1:m]). For all  $m$  considered, from  $m=10$  to  $m=200$ , ACN is found on the surface of the cluster with high probability. The upper panel of Fig. 1 shows an instantaneous configuration of a [1:50] cluster while the lower panel is a plot of  $g_{\text{CM}-\alpha}(r)$ . From this figure it is evident that the ACN molecule is found with high probability at distances of 6–8 Å from the cluster center of mass.

The preferential solvation of ACN near the cluster surface suggests the presence of a free energy minimum, escape from which requires energies greater than typical thermal energies. The free energy or potential of mean force  $W(r)$  as a function of  $r_{\text{ACN}} = |\mathbf{R}_1^{\text{ACN}} - \mathbf{R}_{\text{CM}}|$ , the distance of ACN from the cluster center of mass, is defined by

$$\beta W(r) = -\ln P(r) \propto -\ln \langle \delta(r_{\text{ACN}} - r) \rangle, \quad (6)$$

where  $P(r)$  is the probability of  $r_{\text{ACN}}$  taking the numerical value  $r$ . In order to compute  $W(r)$  in regions of low probability a combination of molecular dynamics and umbrella

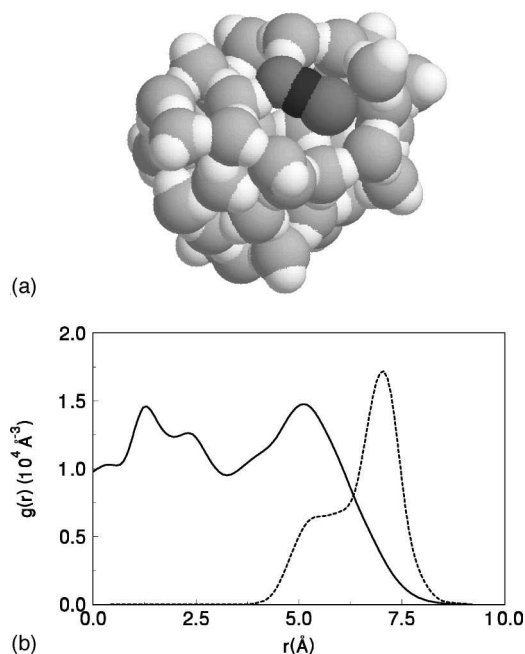


FIG. 1. (a) Instantaneous configuration of the [1:50] cluster showing the ACN molecule on the cluster surface. (b) Spatial correlation function; dashed line ( $\alpha = \text{ACN}$ ); solid line ( $\alpha = \text{W}$ ).

sampling techniques<sup>37</sup> was used. More specifically, the Hamiltonian of the system was augmented with a harmonic potential  $V_{\ell}^h$ ,

$$V_{\ell}^h = \frac{k_{\ell}}{2} (r_{\text{ACN}} - r_{\ell})^2. \quad (7)$$

The values of  $r_{\ell}$  were chosen in the interval  $0 \leq r_{\ell} \leq 6 \text{ \AA}$  and the values of  $k_{\ell}$  were adjusted to obtain considerable overlap between distributions of neighboring windows. The magnitudes of the harmonic restoring forces  $k_{\ell}$  ranged from 2 kcal/mol  $\text{\AA}^{-2}$  for values of  $r_{\ell}$  near the cluster center of mass to 0.5 kcal/mol  $\text{\AA}^{-2}$  for positions near the cluster surface. The reversible work to move the ACN molecule between two points in the cluster can be obtained from the corresponding free energy difference,  $\Delta W$ . The computation of  $\Delta W$  between two points  $r_{\text{ACN}} = r'$  and  $r_{\text{ACN}} = r''$  within the  $\ell$ th window is straightforward and given by

$$\begin{aligned} & W(r'') - W(r') \\ &= \frac{k_{\ell}}{2} [(r'' - r_{\ell})^2 - (r' - r_{\ell})^2] - 2\beta^{-1} \ln \left( \frac{r'}{r''} \right) \\ & \quad - \beta^{-1} \ln \left[ \frac{\langle \delta(r_{\text{ACN}} - r'') \rangle_{V_{\ell}^h}}{\langle \delta(r_{\text{ACN}} - r') \rangle_{V_{\ell}^h}} \right], \end{aligned} \quad (8)$$

where  $\beta^{-1}$  is the Boltzmann constant times the temperature and  $\langle \dots \rangle_{V_{\ell}^h}$  represents a statistical time average obtained with the biased distribution that includes the harmonic potential in Eq. (7). The potential of mean force for a [1:50] cluster is shown in Fig. 2. Perhaps the most interesting feature of this curve is the existence of a double minimum: one near the cluster surface at  $r = 6.7 \text{ \AA}$  and a second located near the cluster center at  $r = 1.5 \text{ \AA}$ . Note that the minimum near

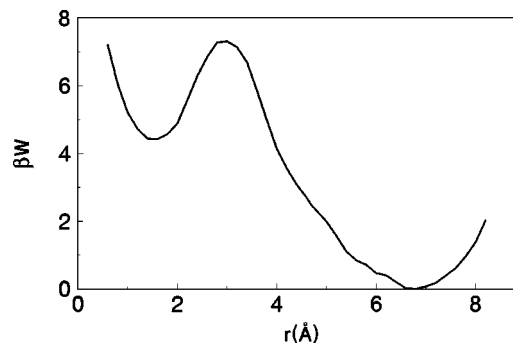


FIG. 2. Potential of mean force as a function of  $r$  for a [1:50] cluster at  $T = 180 \text{ K}$ .

the cluster center is not observed in the data presented in Fig. 1 obtained from unbiased trajectories. The form of the free energy as a function of the radial distance from the cluster center signals the existence of two different solvation structures which we call the surface solvated species  $\mathcal{S}$  and the central solvated species  $\mathcal{C}$ . The free energy barrier for passage between  $\mathcal{C}$  and  $\mathcal{S}$  is located at  $r^{\ddagger} = 3.0 \text{ \AA}$  and has magnitude  $E_f^{\ddagger} = 3k_B T$  for the passage  $\mathcal{C} \rightarrow \mathcal{S}$  and  $E_r^{\ddagger} = 7.4k_B T$  for passage in the opposite direction,  $\mathcal{S} \rightarrow \mathcal{C}$ .

It is interesting to examine the structural and dynamical aspects of the solvation “reaction”



A simple transition state theory (TST) estimate of the forward and reverse rate constants,  $k_i^{\text{TST}} = (\omega_{\mathcal{A}}/2\pi) \exp(-\beta E_i^{\ddagger})$ , with  $i = f, r$  and  $\mathcal{A} = \mathcal{C}, \mathcal{S}$ , yields  $k_f^{\text{TST}} \approx 3 \times 10^{-2} \text{ ps}^{-1}$  and  $k_r^{\text{TST}} \approx 3 \times 10^{-4} \text{ ps}^{-1}$  where the frequency at the  $\mathcal{C}$ -configuration minimum is  $\omega_{\mathcal{C}}/2\pi \approx 0.7 \text{ ps}^{-1}$  and that at the  $\mathcal{S}$  minimum is  $\omega_{\mathcal{S}}/2\pi \approx 0.5 \text{ ps}^{-1}$ . Simulations of a small ensemble of trajectories starting with ACN at the cluster center show passage to the  $\mathcal{S}$  configuration in a few hundred ps. This characteristic time is somewhat longer than the TST prediction. This difference is due to the considerable number of recrossings of the transition-state surface by potentially reactive trajectories, a feature that always leads to a true rate constant that is lower than the TST estimate. None of the 0.5 ns length trajectories ever showed the spontaneous passage  $\mathcal{S} \rightarrow \mathcal{C}$ , consistent with the higher free energy barrier and small rate for this process.

Some insight into the origin of these two solvation species can be gained from an examination of the radial distribution function of water relative to the center of mass of the cluster,  $g_{\text{CM-W}}(r)$ , shown in Fig. 1. This plot shows that the water molecules are distributed inhomogeneously in the cluster, with two regions of maximum probability near  $r = 1.5 \text{ \AA}$  and  $r = 5.5 \text{ \AA}$ , values slightly smaller or comparable to the distances corresponding to the  $\mathcal{C}$  and  $\mathcal{S}$  species, respectively. The local minimum in  $g_{\text{CM-W}}$  near  $r = 3.0 \text{ \AA}$  correlates with the transition state configuration.

The dynamics of the passage between the  $\mathcal{C}$  and  $\mathcal{S}$  configurations is shown in Fig. 3. The trajectories in this figure were initiated with  $r_{\text{ACN}}$  in the  $\mathcal{C}$  configuration and both  $r_{\text{ACN}}$  and the cosine of the angle the ACN dipole makes with the

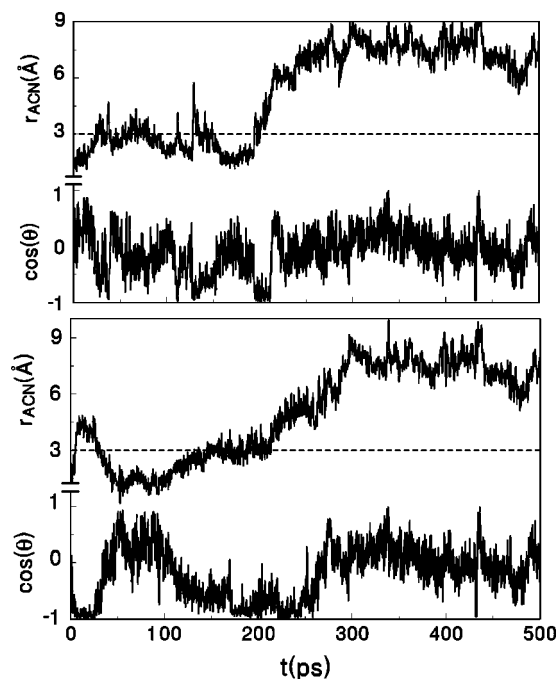


FIG. 3. Two trajectories showing the passage from  $\mathcal{C}$  to  $\mathcal{S}$  configurations for a [1:50] cluster at  $T=180$  K. Direct passage from  $\mathcal{C}$  to  $\mathcal{S}$  (top panel); trajectory showing the transformations  $\mathcal{C} \rightarrow \mathcal{T} \rightarrow \mathcal{C} \rightarrow \mathcal{S}$  (bottom panel). In each panel the upper trajectory is  $r_{\text{ACN}}$  vs time while the lower trajectory is  $\cos \theta$ , where  $\theta$  is the angle between the ACN dipole and the radial vector. The dashed lines represent the transition states.

radial vector,  $\cos \theta = \hat{\boldsymbol{\mu}}_{\text{ACN}} \cdot \hat{\mathbf{r}}_{\text{ACN}}$ , were monitored as a function of time during the reaction  $\mathcal{C} \rightarrow \mathcal{S}$ . In these trajectories one sees two important features: in the upper panel there are clear indications of several unsuccessful attempts of the reaction  $\mathcal{C} \rightarrow \mathcal{S}$  before the final successful reactive event that leads to a stable  $\mathcal{S}$  species at  $t \approx 200$  ps; during these attempts, the solvent buffets the ACN back and forth between the  $\mathcal{C}$  and  $\mathcal{S}$  regions. This is the origin of the deviation from transition state theory discussed above. Secondly, the fact that  $\cos \theta \approx 0$  in the  $\mathcal{C}$  and  $\mathcal{S}$  solvation states indicates that the ACN molecule is on average perpendicular to the radial vector; however, in the transition state region  $\cos \theta \approx -1$  signaling the fact that ACN lies parallel to the radial vector with the dipole pointing inwards (N end of the ACN molecule pointing outwards).

The picture that emerges from these considerations is the following: our results suggest that a clear correlation exists between the regions of stable and unstable solvation of the ACN molecule and the internal spatial correlations of the solvent species.  $\mathcal{C}$  states correspond to an ACN molecule solvated in high density regions of the cluster; on the other hand, the transition state coincides with lower density regions. Finally the profile of  $g_{\text{CM-ACN}}$  in the bottom panel of Fig. 1 shows a shoulder at  $r \approx 5.5$  Å followed by a main peak located at  $r \approx 7$  Å, and suggests the presence of two superficial states with different degrees of solvation. In the stable states, the ACN molecule is preferentially solvated with its dipole normal to the radial vector. In order for the ACN molecule to pass from one stable solvation region to the other, its dipole reorients parallel to the radial vector and

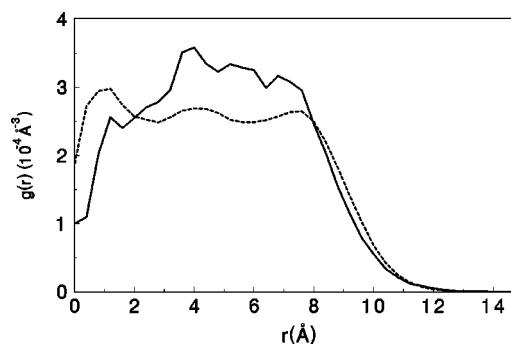


FIG. 4. Radial distribution function  $g_{\text{CM-}\alpha}(r)$  as a function of  $r$  for a [50:1] cluster. Dashed line ( $\alpha=\text{ACN}$ ); solid line ( $\alpha=\text{W}$ ).

then reorients again to the perpendicular direction when it is in the other stable solvation region. This effect is especially clear in the bottom panel of Fig. 3 where rapid passage to the transition state configuration  $\mathcal{T}$  with unsuccessful passage to  $\mathcal{S}$  is then followed by a slower, successful, diffusive passage to  $\mathcal{S}$  on the next attempt. In both cases  $\cos \theta$  shows the orientation effect described above.

The solvation structure of the  $[n:1]$  clusters differs considerably from that of the  $[1:m]$  clusters just described. For sufficiently large clusters, say  $n > 10$ , there was no preferred distance for solvation and thus no distinct solvation species could be identified. Figure 4 shows  $g_{\text{CM-}\alpha}(r)$  for a [50:1] cluster: the presence of a broad, structureless distribution for  $r$  indicates that the interior of the cluster appears as a bulk-like phase for the water molecule solvation. Likewise, the probability distribution  $p(\cos \theta) = p(\hat{\boldsymbol{\mu}}_{\text{W}} \cdot \hat{\mathbf{r}}_{\text{W}})$  (not shown) has a broad distribution indicating a lack of preferential orientation of the water dipole relative to the radial vector.

## B. [2:m] and [n:2] clusters

The analysis of the dynamics of two ACN molecules in a 100-water-molecule cluster ([2:100]) indicates that both solute molecules remain near the cluster surface. However, the radial distribution function  $g_{\text{CC}}(r)$  as a function of the distance between the central C atoms in the ACN pair,  $r = r_{\text{CC}}$ , presented in Fig. 5, shows considerable structure over the entire range of intermolecular distances.

We observe that the most probable configuration corresponds to the solute pair separated by a distance of approxi-

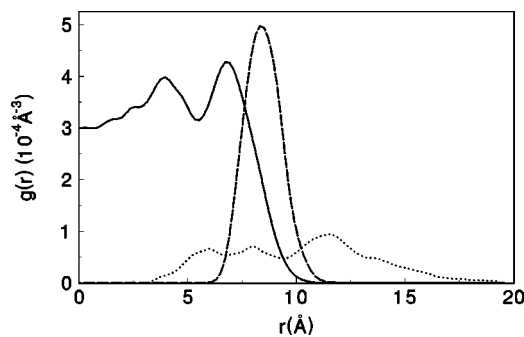


FIG. 5. Radial distribution functions for a [2:100] cluster at  $T=180$  K.  $g_{\text{CC}}(r)$  (dotted line);  $g_{\text{CM-W}}(r)$  (solid line);  $g_{\text{CM-ACN}}(r)$  (dashed line).

TABLE II. Diffusion coefficients ( $\text{\AA}^2 \text{ps}^{-1}$ ) for ACN and water solutes in binary clusters. Center of mass diffusion coefficient ( $D_{\text{CM}}$ ); diffusion coefficient of a solute molecule in the binary cluster [n:m] ( $D_S$ ); diffusion coefficient for a single solute molecule in the [1:50] or [50:1] clusters ( $D_1$ ).

$n(\text{ACN})$	$m(\text{W})$	$T(\text{K})$	$6D_{\text{CM}}$	$6D_S$	$6D_1$
2	50	187	0.07	0.18	0.44
50	2	203	0.43	0.45	0.74

mately 12  $\text{\AA}$ , comparable to the linear dimension of the cluster, with evidence of structural correlations at shorter separations. Thus, the two ACN molecules do not behave as independent molecules in the surface layer, and there is a tendency to form ‘‘dumbbell’’-like configurations with ACN molecules on opposite ends of the cluster. The existence of correlated motion is confirmed by a comparison of the diffusion coefficients of the center of mass of the ACN pair,  $D_{\text{CM}}$ , that of the individual ACN molecules in the pair,  $D_S$ , and  $D_1$ , the diffusion coefficient for a single ACN molecule in the cluster. Estimates of intracluster diffusion coefficients were obtained from the intermediate linear regime of the corresponding root mean square displacements before they reach their limiting plateau values at sufficiently long times. These results are presented in Table II. Note that  $D_{\text{CM}} = D_S/2$  as would be expected for two widely-separated molecules but  $D_1 > D_S$  indicating restricted diffusion for the molecules comprising the pair.<sup>38</sup>

The behavior a water pair in a 100-ACN-molecule cluster ([100:2]) differs from that of the ACN solutes in a [2:100] cluster. In Fig. 6 we plot  $g_{\text{CM-WD}}(r)$ , the radial distribution function of the center of mass of the water dimer,  $\mathbf{R}_{\text{WD}}$ , with respect to the center of mass of the cluster,  $r = r_{\text{WD}} = |\mathbf{R}_{\text{CM}} - \mathbf{R}_{\text{WD}}|$ . From this figure we see that the center of mass of the water-molecule pair is roughly equally likely to be found anywhere in the interior of the cluster. In fact, the  $g_{\text{CM-WD}}$  profile does not differ substantially from that of a water monomer.

Additional information on the nature of the dynamics can be gained from an examination of the trajectories of  $r_{\text{WD}}$  and the internuclear separation between the water molecules,  $r = r_{12} = |\mathbf{R}_{W1} - \mathbf{R}_{W2}|$ . The time variation of these distances is shown in Fig. 7 for a long (6 ns) trajectory. The bound water pair with an internuclear separation of  $r_{12} \approx 3 \text{\AA}$  is easily identified as are the episodes of dissociation of the bound pair. The trajectory of  $r_{\text{WD}}$  exhibits diffusive behavior throughout the cluster. These features are confirmed by the values of the diffusion constants of the water pair and its constituent molecules. From the data in Table II we see that both the water-molecule,  $D_S$ , and pair-center-of-mass,  $D_{\text{CM}}$ , diffusion constants are the same within statistical uncertainty.

Given the existence of a bound water molecule pair, it is interesting to estimate the free energy required for dissociation to ‘‘free’’ water molecules and inquire into the possibility of solvent separated water species. The relevant information is contained in the potential of mean force  $W(r)$  defined by Eq. (6) but now for the pair distance  $r_{12}$ . The mean potential was computed integrating the mean force  $F(r)$  act-

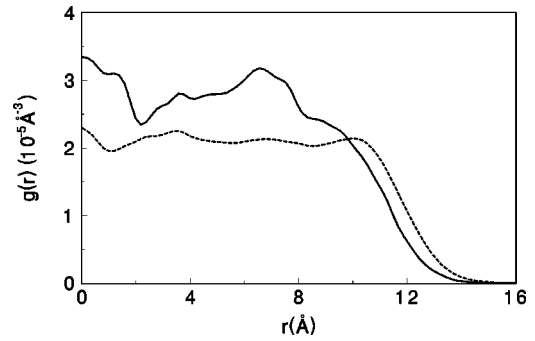


FIG. 6. Radial distribution function  $g_{\text{CM-WD}}$  as a function of  $r$  for a [100:2] cluster at  $T = 180 \text{ K}$  (solid line). The dashed line corresponds to  $g_{\text{CM-ACN}}$  in the same cluster.

ing on each molecule, calculated for the water pair constrained at selected intermolecular distances,  $r$ :

$$F(r) = -\frac{dW(r)}{dr} = -\langle \mathbf{F}_W \cdot \hat{\mathbf{r}} \rangle_r + \frac{2}{\beta r}, \quad (9)$$

where  $\mathbf{F}_W$  represents the total force exerted upon one of the water molecules,  $\hat{\mathbf{r}}_{12} = \hat{\mathbf{r}}$  is a unit vector and  $\langle \dots \rangle_r$  signifies a time average computed using the constrained-reaction-coordinate-dynamics ensemble.<sup>39</sup> The resulting potential of mean force is shown in Fig. 8. We may also estimate  $W(r)$  directly from the histogram of  $r$  in a long unconstrained trajectory; these results are also presented in the figure. The potential of mean force has its first minimum at  $r_{12} = 2.9 \text{\AA}$  corresponding to a ‘‘contact’’ water pair (CWP), a local maximum at  $r = 4.8 \text{\AA}$  corresponding to a transition state configuration, and a second shallow minimum at  $r_{12} = 6.7\text{--}6.8 \text{\AA}$  corresponding to a weakly stable solvent separated water pair (SSWP). The free energy barrier for the reaction  $\text{CWP} \rightarrow \text{SSWP}$  is  $E_f^\ddagger = 7.4 k_B T$ , while that for the reverse reaction  $\text{SSWP} \rightarrow \text{CWP}$  is  $E_r^\ddagger < 1 k_B T$ .

We have also studied the frictional properties of the water pair. The fixed-particle, space-dependent friction coefficient of the pair is related to the time integral of the fluctuations of the fixed-particle force autocorrelation function:

$$\zeta(r) = \beta \langle f(0;r)f(0;r) \rangle \int_0^\infty dt C_F(t;r), \quad (10)$$

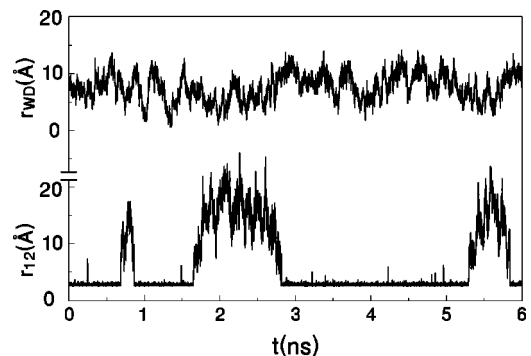


FIG. 7. Trajectories showing the position of the water-pair center of mass  $r_{\text{WD}}$  and the internuclear separation between the water molecules  $r_{12}$  as a function of time for a [100:2] cluster at  $T = 180 \text{ K}$ .

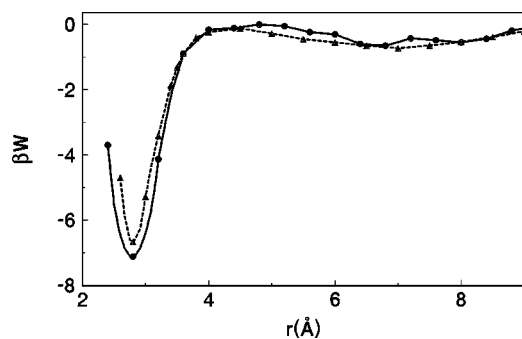


FIG. 8. Potential of mean force  $W(r)$  as a function of  $r$  for a [100:2] cluster at  $T=180$  K. The circles correspond to results obtained by integrating the solvent forces on the constrained water pair; the triangles are results obtained from a histogram of the distance between an unconstrained pair taken from a 6 ns trajectory.

where the normalized force autocorrelation function  $C_F(t;r)$  is

$$C_F(t;r) = \langle f(t;r)f(0;r) \rangle \langle f(0;r)f(0;r) \rangle^{-1}, \quad (11)$$

and the component along the internuclear axis of the solvent fluctuating force  $\mathbf{F}_S$  at a fixed internuclear separation is

$$f(t;r) = \mathbf{F}_S(t;r) \cdot \hat{\mathbf{r}} - \langle \mathbf{F}_S(t;r) \cdot \hat{\mathbf{r}} \rangle. \quad (12)$$

The autocorrelation function  $C_F(t;r)$  is plotted in Fig. 9 as a function of time for several values of  $r$ . From this figure we see that the force autocorrelation takes two forms: one for  $r$

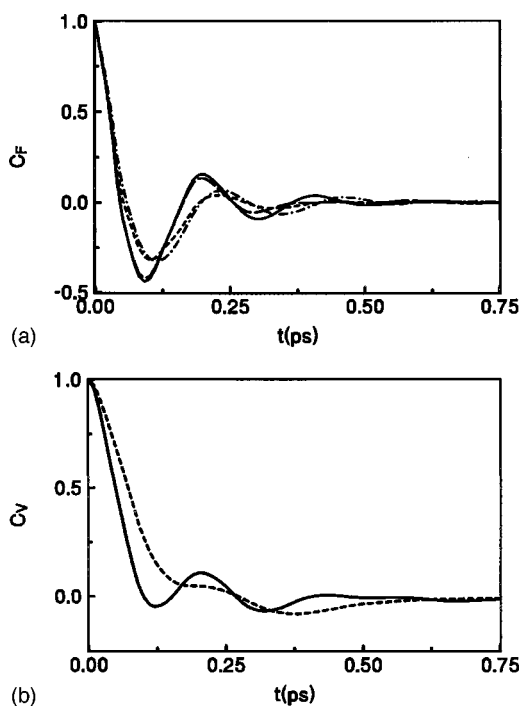


FIG. 9. (a) Force autocorrelation function  $C_F(t;r)$  as a function of  $t$  for  $r = 2.8$  and  $3.6$  Å (short dashed and dot-dashed lines) and  $r = 4.0$  and  $7.0$  Å (long dashed and solid lines) for a [100:2] cluster at  $T=230$  K. Results at short distances are almost indistinguishable on the scale of the figure. (b) Velocity autocorrelation function as a function of  $t$  for  $r = 2.8$  Å (dashed) and  $7.0$  Å (solid).

values in the vicinity of the water contact water pair and the other for distances  $r > 4$  Å, where a solvent molecule is wedged between the solute pair.

We note that the different character of these two spatial regimes is also reflected in the structure of the velocity autocorrelation function. In the bottom panel of Fig. 9 we show results for  $C_V(t)$ ,

$$C_V(t;r) = \frac{\langle v(t;r)v(0;r) \rangle}{\langle v^2(0;r) \rangle}, \quad (13)$$

where  $v(t;r) = \mathbf{V}_{CM}(t;r) \cdot \hat{\mathbf{r}}$  is the projected velocity of the center of mass of the constrained water dimer along the internuclear direction.

The space-dependent friction coefficient given by Eq. (10) increases as  $r$  decreases until  $r \approx 3$  Å, after which it ceases to increase. (The data are not sufficiently accurate to deduce the details of its structure for small  $r$ .) A simple hydrodynamic model that accounts for the Oseen interactions between the two particles yields a friction coefficient of the form,<sup>40</sup>

$$\zeta(r) = \frac{\zeta_1}{2} [1 + \zeta_1 \hat{\mathbf{r}} \cdot \mathbf{T}(r) \cdot \hat{\mathbf{r}} + \mathcal{O}(T^2)], \quad (14)$$

where  $\zeta_1$  is the friction coefficient for a single water molecule and the Oseen tensor is  $\mathbf{T}(r) = (1 + \hat{\mathbf{r}}\hat{\mathbf{r}})/8\pi\eta r$ , with  $\eta$  the viscosity. This formula predicts that the friction should increase and even diverge as  $r$  decreases to zero. A kinetic theory calculation of the friction that accounts for static structural three-body correlations among the two solute particles and a solvent particle yields a friction coefficient that rises as  $r$  decreases but for  $r$  sufficiently small the friction falls as a result of collisional screening.<sup>41</sup> Due to the strong oscillations of the force autocorrelation function that make the estimation of the friction difficult, we cannot distinguish between the hydrodynamic and microscopic contributions but the fact that the friction ceases to rise is suggestive of the existence of the influence of structural correlations on the pair friction, also evident in the plots of the force autocorrelation function.

#### IV. CONCENTRATED CLUSTERS

The density fluctuations in larger and more concentrated ACN-W mixed clusters also show a distinct behavior depending on which component is in excess. Consider aggregates composed of 50 ACN and 200 W molecules. Figure 10 is a snapshot of a such a [50:200] cluster configuration exhibiting few signs of mixing between the components. The cluster has a roughly spherical shape with the ACN solute molecules distributed over the surface of a water nucleus. An estimate of the size of the cluster can be obtained from the average gyration radius,  $\mathcal{R}$ , defined as

$$\mathcal{R}^2 = \frac{1}{N_{ACN} + N_W} \left\langle \sum_{\alpha,i} (\mathbf{R}_{CM} - \mathbf{R}_i^\alpha)^2 \right\rangle. \quad (15)$$

For spherical aggregates, the radius of the cluster can be approximated by  $\sqrt{5/3}\mathcal{R} = 12.5$  Å. An inspection of  $g_{CM-\alpha}(r)$  for  $\alpha = ACN$  and  $W$ , shown in the top panel of

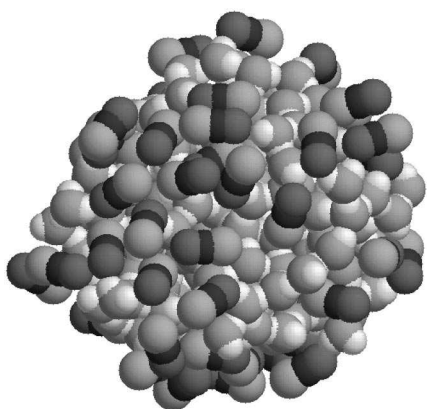


FIG. 10. Instantaneous configuration of the [50:200] cluster showing the ACN molecules partially covering an internal water subcluster.

Fig. 11, confirms this observation: the distribution of ACN molecules exhibits a Gaussian-type profile centered at  $r = 12.4 \text{ \AA}$ , a distance quite close to the estimate based on  $\mathcal{R}$ . This value also coincides with the position of the surface of the water subcluster. Structural correlations within the water subcluster shown in the  $g_{\text{CM-W}}(r)$  plot are much less evident.

The nature of the arrangement of the solute molecules on the cluster surface can be deduced from an inspection of the solute pair correlation function (Fig. 11, bottom panel). We observe a prominent peak at  $r \approx 4.5 \text{ \AA}$ , a secondary and much smaller maximum at  $r \approx 8 \text{ \AA}$  and no perceptible structure beyond  $10 \text{ \AA}$ . The similarities between this long range behavior and the spatial correlations between points randomly

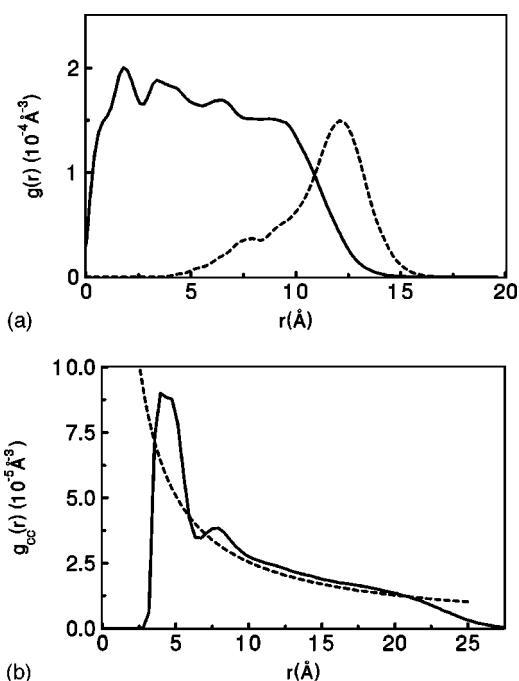
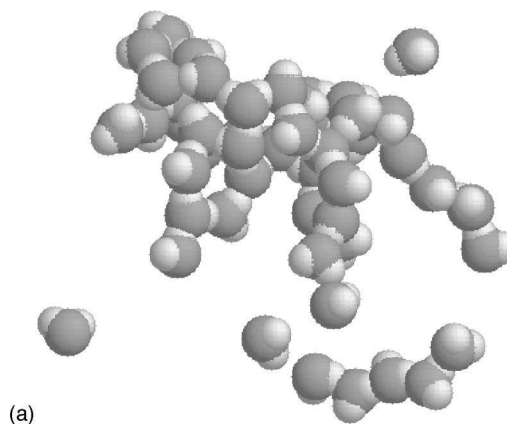
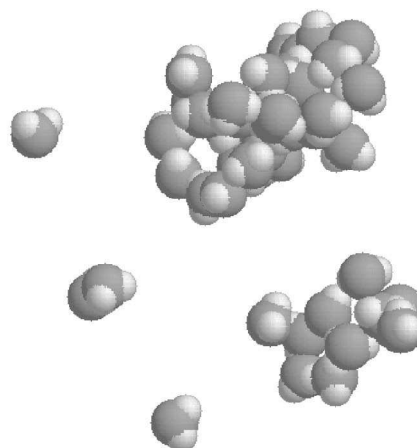


FIG. 11. (a) Radial distribution function  $g_{\text{CM-a}}(r)$  as a function of  $r$  for a [50:200] cluster. Same labeling as Fig. 1. (b) Radial distribution function  $g_{\text{CC}}(r)$  as a function of  $r$  for a [50:200] cluster. The dashed line corresponds to the distribution of points randomly distributed on the surface of a sphere of radius  $12.5 \text{ \AA}$ .



(a)



(b)

FIG. 12. (a) and (b) show two water subcluster configurations in a [200:50] cluster corresponding to “dendritic” and compact structures, respectively. The ACN molecules are not shown.

distributed on the surface of a sphere—also shown in the figure—indicate that the ACN molecules tend to distribute homogeneously over the surface of the water nucleus. They do not form compact “island” structures and strong correlations persist only over distances of a few angstroms. The fact that  $D_{\text{CM}}$  for the ACN molecules is very small is also consistent with these observations; the root-mean-square displacement of the center of mass of the ACN molecules levels off to a constant plateau value of approximately  $1.4 \text{ \AA}^2$  after a short initial inertial interval showing no evidence of an intermediate linear regime.

The situation changes dramatically when one considers the inverse case, i.e., clusters composed of 200 ACN and 50 W molecules ([200:50]). Perhaps the most direct way to visualize these changes is from an inspection of several hundreds of configurations generated along the molecular dynamics trajectory (cf. Fig. 12). The trajectory shows clear signs of mixing of the components. Although the overall shape of the cluster is spherical, in the vast majority of these configurations the water molecules form irregularly-shaped domains whose sizes and shapes fluctuate strongly. Occasionally, a water subcluster will fragment into smaller aggregates that diffuse independently throughout the solvent until they eventually re-encounter each other and recombine to form a single aggregate. The characterization of shape fluc-

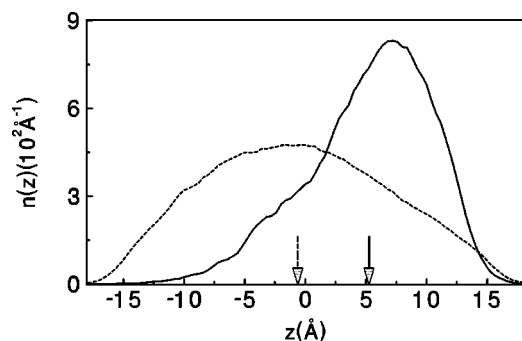


FIG. 13. Density profile along the  $z$ -axis (see text) for W (solid line) and ACN (dashed line). The arrows indicate the positions of the centers of mass of the ACN and W subclusters.

tuations is not straightforward since it involves collective modes of many solute molecules. Several correlation functions will be used to probe this structure.

To obtain information about the global structure consider the distribution of the different species within the aggregate. Figure 13 shows plots for the density  $n^\alpha(z)$  defined as:

$$n^\alpha(z) = \frac{1}{N_\alpha} \left\langle \sum_i^{N_\alpha} \delta(Z_i^\alpha - z) \right\rangle, \quad (16)$$

where  $Z_i^\alpha$  is the  $z$ -component of  $\mathbf{R}_i^\alpha$ . Here, the  $z$  axis has been chosen along the vector  $\mathbf{R}_{\text{CM}}^W - \mathbf{R}_{\text{CM}}^{\text{ACN}}$  that joins the centers of mass of the W and ACN components and is centered at  $\mathbf{R}_{\text{CM}}$ . Two important observations can be extracted from these curves: (i) the linear dimensions of the aggregate are close to 35 Å, a result that agrees reasonably well with the estimate computed from the average gyration radius  $2 \times \sqrt{3}/5R = 32.2$  Å and corroborates the earlier observation that the overall shape of the cluster is spherical. (ii) This feature contrasts sharply with the distribution of the solute particles within the cluster. This distribution is nonspherical and displaced with respect to  $\mathbf{R}_{\text{CM}}$ . Reasonable estimates of the shape anisotropy and the magnitude of the size fluctuations can be obtained from comparing its principal moments of inertia:  $(\langle I_3 \rangle / \langle I_1 \rangle)^{1/2} = 1.4$  and  $(\langle I_2 \rangle / \langle I_1 \rangle)^{1/2} = 1.2$ , and by computing the corresponding standard deviations  $\langle (\delta I_i)^2 \rangle^{1/2} \langle I_i \rangle^{-1}$  which are  $\approx 0.15$  for all  $i$ . The average displacement of the water center of mass with respect to that of the cluster can be obtained by simply integrating  $n^W(z)$  as follows:

$$\langle |\mathbf{R}_{\text{CM}}^W - \mathbf{R}_{\text{CM}}| \rangle = \int n^W(z) z dz = 5.3 \text{ \AA}. \quad (17)$$

The analysis of the average pair structure provides additional details about spatial correlations between the solute molecules. In the top panel of Fig. 14 we plot  $g_{WW}(r)$  for a [200:50] cluster. The curve shows the usual peaks that characterize the short-distance ordering of compact structures and a tail that decays on distances of the order of  $r \approx 20$  Å. The direct comparison of this profile with that for a pure 50-molecule water cluster is instructive. The evident differences in the magnitudes of the peaks for [200:50] and [0:50] clusters is indicative of the reduction in the number of water

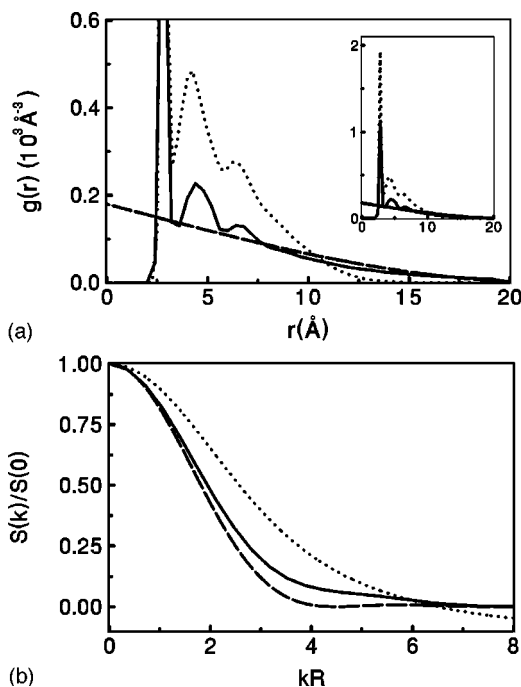


FIG. 14. (a) Radial distribution function  $g_{WW}(r)$  as a function of  $r$  for a [200:50] cluster (solid line); for a [0:50] (dotted line). The dashed line corresponds to the distribution of ideal points within a sphere of radius  $R = 10$  Å. (b) Water-water structure factor  $S(k)$ . Same labeling as the top panel.

water nearest neighbors in the former case; the areas under the main peaks are 2.7 and 3.8, respectively. Despite these differences in magnitude, the locations of these peaks are almost identical indicating that similar connectivity mechanisms through hydrogen bonding exist and that there are only minor disruptions of the distances between neighboring water molecules. Of course, due to conservation of mass, the reduction of the local density at short distances around a given water molecule should lead to longer length scale structure in the water-water pair correlation function. To characterize these long range spatial correlations, in Fig. 14 we have also included results for  $g_{\text{id}}(r)$ , the distribution of ideal, i.e., noninteracting, points within a sphere of size comparable to the maximum correlation length of  $g_{WW}$ . Equivalent information can be extracted from the small-wave-vector limit of the corresponding Fourier density spectra shown in the lower panel of Fig. 14. The evident differences between the two sets of curves in  $r$  and  $k$  spaces, suggest the persistence of non-negligible spatial correlations over distances comparable to the size of the aggregate.

A partial explanation for this behavior is as follows: we have already noted that the simulation results suggest incipient mixing of the two components. Starting from a compact water subcluster, interactions with the solvent induce large fluctuations in the ACN-W interface eventually leading to a “dendriticlike” structure. Often, the original water subcluster fragments into smaller subclusters ranging in size from water monomers to aggregates containing roughly 10–15 molecules that “survive” for periods of several picoseconds before recombining. These observations suggest that the long-distance behavior of  $g_{WW}(r)$  is due to the combination

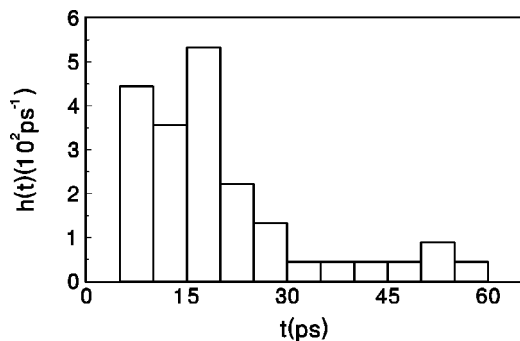


FIG. 15. Histogram for the characteristic times for fragmentation/recombination processes of water subclusters in [200:50] aggregates.

of spatial correlations within a “dendriticlike” water subcluster as well as those between different subcluster fragments.

The magnitude of solute cluster-fragment diffusion and the extent of the spatial confinement provided by the ACN molecules are important factors determining the time scale for the water subcluster fragmentation-recombination process. An estimate of the characteristic time may be obtained as follows. Using a criterion based on a minimum connectivity distance  $d_c$  between water molecules, we have computed the number of water subclusters present at time  $t$ . Variations in the water subcluster population that occurred over time periods less than a minimum value,  $\tau_{\min}$ , were not taken into account in order to avoid changes in the cluster population that arose from small fluctuations in the interparticle distances around  $d_c$  that did not correspond to real fragmentation or recombination processes. Once these high-frequency contributions were filtered out, a histogram of the survival probability of the water subcluster population was constructed. Several choices of  $d_c$  and  $\tau_{\min}$  were considered. The histogram  $h(t)$  for  $d_c = 3.8 \text{ \AA}$  and  $\tau_{\min} = 2.5 \text{ ps}$  is shown in Fig. 15. This choice yielded results which were stable with respect to reasonable variations of these parameters. From the histogram the average time interval between fragmentation and/or recombination was estimated to be approximately 20 ps, providing an estimate of the average time for the interconversion dynamics of the solute subclusters.

## V. CONCLUSION

The structural and dynamical properties of polar-molecule, liquid-state nanoclusters described in this paper illustrate some of the unusual properties of matter on these length scales. These distinctive properties have implications for cluster solvation, reaction dynamics in clusters and the possibility of finite-size analogs of binary fluid phase transitions.

For the entire temperature range where liquidlike binary clusters are stable, no regime of complete mixing was found. All mixed clusters showed some degree of segregation. The existence of a free surface and surface forces manifest themselves in a number different ways in binary polar clusters. Not only do they lead to the differentiation between surface and cluster-interior solvation species as might be expected, but they also induce strong structural correlations in the clus-

ter interior, which are much more evident in water aggregates than in aggregates of acetonitrile. These correlations in turn can promote the formation of (less stable) solvation structures such as those seen for ACN solutes in water clusters. The different types of solvation may be regarded as “chemical” species and their reaction dynamics can be studied as activated rate processes. However, considering the surface-to-volume ratio, even the largest systems of this study may be considered to lie in the small-scale regime and one should expect that the solvation structure will gradually change in water clusters which are still mesoscopic in size but contain several thousands of molecules. In such cases internal solvation should become entropically favored, approaching the limiting macroscopic regime where complete mixing is observed.

The solvation structure and dynamics need not be simple, as observed for concentrated water solute molecules in ACN clusters. In these cases, the spatial confinement induces only orientational correlation on the cluster surface and no signs of dipolar circulation patterns similar to those found in Stockmayer clusters could be observed.<sup>42</sup> Water molecules do not form compact aggregates but instead form irregular domains that fragment and recombine yielding large local water concentration fluctuations interior to the cluster, akin to those seen in binary fluids near the consolute point. From a different although equivalent perspective, the large fluctuations of the W-ACN interface that signal the approach of the mixed regime could be regarded as the effect of a large external ACN shell on an internal 50-water-molecule nucleus. In the early stages of this mixing process the original compact water subcluster evolves into a highly irregular fingerlike structure that invades solvent domains. As a direct consequence, the hydrogen-bonded, three-dimensional network weakens and thermal fluctuations and interactions with the solvent can be strong enough to generate fragments that survive for time periods of the order of a few tens of picoseconds. Of course the recombination of the smaller fragments is just a consequence of the spatial confinement and should be absent in the corresponding macroscopic phases. We finally remark that all attempts to thermally force the mixing process of both components were unsuccessful since rapid evaporation of the cluster occurred as the temperature was raised beyond  $T \approx 250 \text{ K}$ .

## ACKNOWLEDGMENTS

Partial financial support from Fundaci3n Antorchas of Argentina is very much appreciated. D.L. is a member of Carrera del Investigador Científico del CONICET (Argentina). The research of R.K. was supported in part by a grant from the Natural Sciences and Engineering Research Council of Canada.

<sup>1</sup>A. W. Castleman, Jr. and R. G. Keese, *Chem. Rev.* **86**, 589 (1986); *Annu. Rev. Phys. Chem.* **37**, 525 (1986); *Science* **241**, 36 (1988); A. W. Castleman, Jr. and S. Wei *Annu. Rev. Phys. Chem.* **45**, 685 (1994).

<sup>2</sup>See, *Physics and Chemistry of Finite Systems: From Clusters to Crystals*, edited by P. Jena, S. N. Khana, and B. K. Rao (Kluwer, Dordrecht, 1992).

<sup>3</sup>See papers in *Small Particles and Inorganic Clusters*, in *Proc. ISSPIC8*, edited by H. H. Andersen (Springer, Berlin, 1997).

<sup>4</sup>R. S. Berry, J. Jellinek, and G. Natanson, *Phys. Rev. A* **30**, 919 (1984).

- <sup>5</sup>H. Reiss, G. Rong, and A. Ward, *J. Phys. Chem.* **92**, 7241 (1988).
- <sup>6</sup>R. S. Berry, T. L. Beck, H. L. Davis, and J. Jellinek, *Adv. Chem. Phys.* **90**, 75 (1988).
- <sup>7</sup>M. Y. Hahn and R. L. Whetten, *Phys. Rev. Lett.* **61**, 1190 (1988).
- <sup>8</sup>J. Bösigler and S. Leutwyler, *Phys. Rev. Lett.* **59**, 1895 (1987).
- <sup>9</sup>P. Labastie and R. L. Whetten, *Phys. Rev. Lett.* **65**, 1567 (1990).
- <sup>10</sup>H.-P. Cheng, X. Li, R. L. Whetten, and R. S. Berry, *Phys. Rev. A* **46**, 791 (1992).
- <sup>11</sup>For a recent review of advances in the area see, for example, *Reaction Dynamics in Clusters and Condensed Phases*, edited by J. Jortner, R. D. Levine, and B. Pullman (Kluwer, Dordrecht, 1994).
- <sup>12</sup>B. D. Kay, V. Hermann, and A. W. Castleman, Jr., *Chem. Phys. Lett.* **80**, 469 (1981).
- <sup>13</sup>O. Cheshnovsky and S. Leutwyler, *Chem. Phys. Lett.* **121**, 1 (1985).
- <sup>14</sup>R. Knochenmuss, O. Cheshnovsky, and S. Leutwyler, *Chem. Phys. Lett.* **144**, 317 (1988).
- <sup>15</sup>S. Consta and R. Kapral, *J. Chem. Phys.* **101**, 10 908 (1994).
- <sup>16</sup>S. Consta and R. Kapral, *J. Chem. Phys.* **104**, 4581 (1996).
- <sup>17</sup>D. Laria, R. Kapral, D. Estrin, and G. Ciccotti, *J. Chem. Phys.* **104**, 6560 (1996).
- <sup>18</sup>D. Scharf, J. Jortner, and U. Landman, *J. Chem. Phys.* **88**, 4273 (1988).
- <sup>19</sup>L. Perera and F. Amar, *J. Chem. Phys.* **93**, 4884 (1990).
- <sup>20</sup>G. Markovich, S. Pollack, R. Giniger, and O. Cheshnovsky, *J. Chem. Phys.* **101**, 9344 (1994).
- <sup>21</sup>M. Re and D. Laria, *J. Chem. Phys.* **105**, 4584 (1996).
- <sup>22</sup>P. Xia and L. A. Bloomfield, *Phys. Rev. Lett.* **70**, 1779 (1993).
- <sup>23</sup>H. Hakkinen, R. N. Barnett, and U. Landman, *Chem. Phys. Lett.* **232**, 79 (1995); R. N. Barnett, H.-P. Cheng, H. Hakkinen, *J. Phys. Chem.* **99**, 7731 (1995).
- <sup>24</sup>L. Parera and M. L. Berkowitz, *J. Phys. Chem.* **95**, 1954 (1991); **96**, 8288 (1992); **99**, 4236 (1993).
- <sup>25</sup>D. Lu and S. J. Singer, *J. Chem. Phys.* **105**, 3700 (1996).
- <sup>26</sup>D. Laria and R. Fernández-Prini, *J. Chem. Phys.* **102**, 7664 (1995).
- <sup>27</sup>F. Amar and B. J. Berne, *J. Phys. Chem.* **88**, 6720 (1984).
- <sup>28</sup>L. Perera and F. Amar, *J. Chem. Phys.* **90**, 7354 (1989).
- <sup>29</sup>Q. Liu, J.-K. Wang, and A. H. Zewail, *Nature (London)* **364**, 427 (1993).
- <sup>30</sup>A. S. Clarke, R. Kapral, B. Moore, G. Patey, and X.-G. Wu, *Phys. Rev. Lett.* **70**, 3283 (1993).
- <sup>31</sup>A. S. Clarke, R. Kapral, and G. Patey, *J. Chem. Phys.* **101**, 2432 (1994).
- <sup>32</sup>H. J. C. Berendsen, J. P. M. Postma, W. F. Von Gunsteren, and J. Hermans, *Intermolecular Forces* (Reidel, Dordrecht, 1981).
- <sup>33</sup>D. M. F. Edwards, P. A. Madden, I. R. McDonald, *Mol. Phys.* **51**, 1141 (1984).
- <sup>34</sup>S. Nosé, *Mol. Phys.* **52**, 255 (1984).
- <sup>35</sup>M. P. Allen and D. J. Tildesley, *Computer Simulations of Liquids* (Clarendon, Oxford, 1987).
- <sup>36</sup>J. P. Ryckaert, G. Ciccotti, and H. J. C. Berendsen, *J. Comput. Phys.* **23**, 327 (1977).
- <sup>37</sup>G. Torrie and J. P. Valleau, *J. Comput. Phys.* **23**, 187 (1977).
- <sup>38</sup>A simple model based on the Kirkwood-Riseman theory predicts that the diffusion of the center of mass of a set of  $N$ -monomers dissolved in a continuum of viscosity  $\eta$ , can be approximated by  $D_{CM} \approx D_s/N + (1/6\pi\eta N^2) \sum_{i \neq j} \langle 1/r_{ij} \rangle$ . See, for example, H. Yamakawa, *Modern Theory of Polymer Solutions* (Harper and Row, New York, 1971), Chap. VI.
- <sup>39</sup>E. A. Carter, G. Ciccotti, J. T. Hynes, and R. Kapral, *Chem. Phys. Lett.* **156**, 472 (1989).
- <sup>40</sup>R. Kapral, *Chem. Phys. Lett.* **86**, 1259 (1982).
- <sup>41</sup>R. I. Cukier, R. Kapral, and J. R. Mehafeey, *J. Chem. Phys.* **73**, 5254 (1980).
- <sup>42</sup>H. B. Lavender, K. A. Iyer, and S. J. Singer, *J. Chem. Phys.* **101**, 7856 (1994).